

Geometric local structure at the Mn site in charge-ordered mixed valence manganites

M. C. Sánchez,^{a*} J. García,^a G. Subías,^a J. Blasco^a and M. G. Proietti^a

^aInstituto de Ciencia de Materiales de Aragón, C.S.I.C.-Universidad de Zaragoza, CL Pedro Cerbuna 12, 50009 Zaragoza, Spain.
Email: csanchez@posta.unizar.es

An extensive study of Mn K-edge absorption spectroscopy has been carried out in $\text{La}_{1-x}\text{Ca}_x\text{MnO}_3$ and $\text{Tb}_{1-x}\text{Ca}_x\text{MnO}_3$ ($x=0, 0.33, 0.5, 0.67, 1$) series as a function of temperature. The EXAFS analysis for the charge ordering compounds ($x \geq 0.5$) shows the presence of a static distortion of the MnO_6 octahedron in the whole temperature range. However, this local distortion is lower than the distortion found for Jahn-Teller compounds. Magnetoresistive compounds ($x=0.33$) show a regular octahedron in the low temperature metallic phase. Instead, no changes are found for the first coordination shell (Mn-O) across the charge ordering transition while Mn-Mn distribution shows minor variations with the temperature. The structural analysis of the second coordination shell suggests that the Mn-O-Mn angle is the most relevant parameter to describe the electric and magnetic behaviour of these compounds.

Keywords: EXAFS, Charge-ordering, Giant magnetoresistance

1. Introduction

Mixed-valence manganese/rare earth oxides show a huge variety of physical properties: giant magnetoresistance, magnetic or electrical field induced structural changes and different kind of magnetic arrangements (Coe *et al.*, 1999). The end-members of the series are antiferromagnetic insulators with a magnetic structure of A-type (LaMnO_3), G-type (CaMnO_3) and incommensurate for TbMnO_3 , respectively. The replacement of La by Ca leads to a formal oxidation from Mn^{3+} into Mn^{4+} . Intermediate compositions of $\text{La}_{1-x}\text{Ca}_x\text{MnO}_3$ ($0.2 \leq x \leq 0.5$) series develop a metallic state coupled to a long-range ferromagnetic ordering. The double exchange mechanism is considered to be responsible of such behaviour. However, an insulator state coupled to an antiferromagnetic ground state is observed for $x \geq 0.5$. This insulator state has been explained by a charge ordering of Mn^{3+} and Mn^{4+} but recent spectroscopic studies are casting doubts on this model (García *et al.*, 2000). $\text{Tb}_{1-x}\text{Ca}_x\text{MnO}_3$ series, instead, does not achieve a long range ferromagnetic state for any x value. Only a spin-glass behaviour is observed for $x=0.33$ while the so-called charge-ordering state is more stable, appearing at room temperature for the $x=0.5$ compound (Blasco *et al.*, 1997). The local structure determination, in particular, the possible relationship between the local vibration modes and the electron motion is very important to understand the behaviour of these materials. Several experiments have been used for determining the local structure of the Mn atom. Extended X-ray Absorption Fine Structure (EXAFS) has been widely used by several authors (Tyson *et al.*, 1996; Meneguini *et al.*, 1997; Booth *et al.*, 1996; *ibid* 1998; Lanzara *et al.*, 1998; Subías *et al.*, 1998). In this paper, we extend our previous work on $\text{La}_{1-x}\text{Ca}_x\text{MnO}_3$ and $\text{Tb}_{1-x}\text{Ca}_x\text{MnO}_3$ ($x \leq 0.33$) samples (Subías *et al.*, 1998) to the so-called charge-ordered compounds. The variation of the local

structure as a function of doping (x) and, for each sample, as a function of temperature is presented for the whole $\text{La}_{1-x}\text{Ca}_x\text{MnO}_3$ and $\text{Tb}_{1-x}\text{Ca}_x\text{MnO}_3$ series. Second-shell analysis of the EXAFS spectra has allowed us to determine the Mn-O-Mn angle and its evolution crossing the different phase transitions. This parameter seems to be the control key for the electrical transport properties, as it has been proposed. Moreover, the comparison between the different series has allowed us to correlate changes in the Mn local structure at different doping ratios and at different magnetic and electric phases.

2. Experimental

Samples have been prepared following conventional procedures. The synthesis, electrical and magnetic characterisations are described elsewhere (Blasco *et al.*, 2000; Ibarra *et al.*, 1997). The X-ray absorption experiments were carried out at the beam line BM29 at E.S.R.F. in Grenoble. The storage ring operated with an electron beam of 6 GeV with a maximum stored current of about 190 mA. The energy range of the monochromatized X-rays was 4–27 KeV provided by a fixed-exit-beam double crystal monochromator using Si (111). Silicon photodiodes were used to detect the incident and transmitted flux, providing a full linear energy response. The energy resolution, $\Delta E/E$, was estimated to be about 2×10^{-4} . Harmonic rejection was achieved by a slight detuning of the two crystals from the parallel alignment. The X-ray absorption spectra were measured in the transmission mode. Spectra were recorded above and below room temperature by means of a helium cryostat and a controlled temperature furnace, respectively. Pellets prepared with boron nitride in order to optimise the thickness were used.

Room temperature spectra are identical to those previously reported (Subías *et al.*, 1997, 1998). The extraction of EXAFS data was performed using standard procedures. The k -weighted spectra were Fourier transformed from k to R space in the range $3.5\text{--}12.5 \text{ \AA}^{-1}$.

3. Results and discussion

3.1 First shell analysis

The first-shell EXAFS contribution was extracted by Fourier Filtering spectra between 1 and 2 \AA . The information about the Mn-O bond was obtained by least square fitting of the k -weighted filtered spectra in the range $3.5 < k < 12.5 \text{ \AA}^{-1}$. The Mn-O pair signal extracted from the experimental CaMnO_3 spectrum at room temperature is used as reference signal. Statistical errors in the Debye-Waller (DW) factors are estimated from the best residual factor, corresponding to a 95% confidence interval. Best fit results were obtained for two initial conditions: (1) a Mn atom surrounded by six oxygen atoms at a fixed interatomic Mn-O distance; (2) a tetragonal distorted Mn atom with two different Mn-O interatomic distances (fixed coordination numbers 4 and 2). The results show that the second fit is better than the one distance fit for LaMnO_3 . For the rest of samples, the one shell fit is better from the statistical point of view. However, both fits are in agreement with a large spread of interatomic distances, as deduced from the large DW factors found. In order to compare the data at different doping ratios and at different temperatures, we will focus on the one shell fit data in the following.

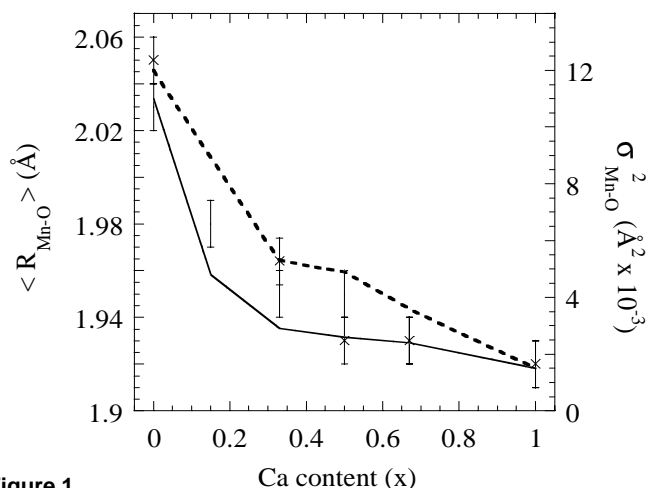


Figure 1. Interatomic Mn-O distances (points) and DW factors (lines) at room temperature for $\text{La}_{1-x}\text{Ca}_x\text{MnO}_3$ (circles and continuous line) and $\text{Tb}_{1-x}\text{Ca}_x\text{MnO}_3$ (crosses and broken line) series as a function of the doping ratio x . Estimated errors for the distances are ± 0.01 Å, whereas for the DW factors are $\pm 0.2 \times 10^{-3} \text{Å}^2$ except for the samples with $x=0$ ($\pm 2 \times 10^{-3} \text{Å}^2$) and $\text{Tb}_{0.67}\text{Ca}_{0.33}\text{MnO}_3$ ($\pm 0.4 \times 10^{-3} \text{Å}^2$) where the two-shell fit is needed.

The average Mn-O interatomic distances and DW factors at room temperature as a function of the valence state (measured by redox titration) for the different series are shown in fig 1. The same average Mn-O distance is obtained for samples with the same formal Mn^{4+} content, independently of the series. The Mn-O distance for compounds with mixed valence state can not be obtained as a linear interpolation between the values corresponded to $\text{La}(\text{Tb})\text{MnO}_3$ and CaMnO_3 . This fact suggests that the MnO_6 local geometry can not be described as a mixture of formal Mn^{3+} and Mn^{4+} oxygen octahedra. We would like to note our attempts to use as references for the Mn-O EXAFS contribution of intermediate compounds, the experimental spectra of $\text{La}(\text{Tb})\text{MnO}_3$ and CaMnO_3 . No reasonable fits were obtained using these two components. On the other hand, the DW factor decreases with the Mn oxidation state in agreement with the reduction of the distortion of the MnO_6 octahedron. We notice a

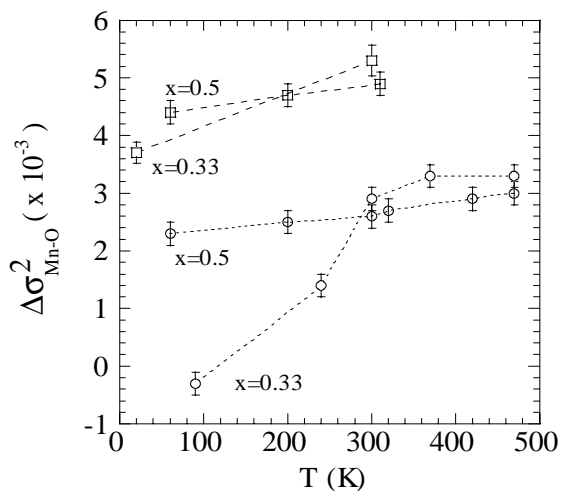


Figure 2. DW factors of the Mn-O first coordination distance of $\text{La}_{1-x}\text{Ca}_x\text{MnO}_3$ (circles) and $\text{Tb}_{1-x}\text{Ca}_x\text{MnO}_3$ (squares) for $x=0.33$ and $x=0.5$, as a function of temperature. DW values are relative to the CaMnO_3 DW factor.

higher distortion for the Tb-Ca series than for the La-Ca series in agreement with the lower ionic radius of Tb^{3+} .

Best fit results of the EXAFS spectra as a function of temperature show that the DW factor is the relevant parameter, since the interatomic Mn-O distances remain nearly constant along these series in the whole temperature range. The comparison of the temperature evolution of the DW factors for the $\text{La}_{1-x}\text{Ca}_x\text{MnO}_3$ ($x=0.33$ and 0.5) and $\text{Tb}_{1-x}\text{Ca}_x\text{MnO}_3$ ($x=0.33$ and $x=0.5$) samples is shown in fig 2. The Tb compounds show larger DW factors than the La compounds for all the temperatures, in agreement with the more distorted crystallographic structure of the Tb series. Samples with $x=0.5$ show a DW factor which is independent of the temperature. As the local distortion of the charge ordering phase, observed by X-ray and neutron diffraction (Radaelli *et al.*, 1995; *ibid.*, 1997; Blasco *et al.*, 1997), remains in the whole temperature range, this distortion must be dynamic in the high temperature (paramagnetic) phase. For $x=0.33$ samples, instead, the temperature evolution of the DW factor observed for the Tb sample is completely different to that found for the La sample. $\text{Tb}_{0.66}\text{Ca}_{0.33}\text{MnO}_3$ shows a gradual increase of the DW factor with increasing the temperature, according to a standard thermal evolution. On the other hand, $\text{La}_{0.67}\text{Ca}_{0.33}\text{MnO}_3$ shows a discontinuous change at the metal-insulator phase transition. The local distortion in the metallic-ferromagnetic phase is similar to that of the CaMnO_3 compound, i.e. we can say that a regular MnO_6 octahedron is characteristic of the low temperature phase of this compound. Fig. 3 shows the DW factors as a function of the reduced temperature for several $x=0.33$ samples. The same behavior is observed for all the studied samples independently of the phase transition temperature, corroborating the lack of distortion in the metallic-ferromagnetic phase.

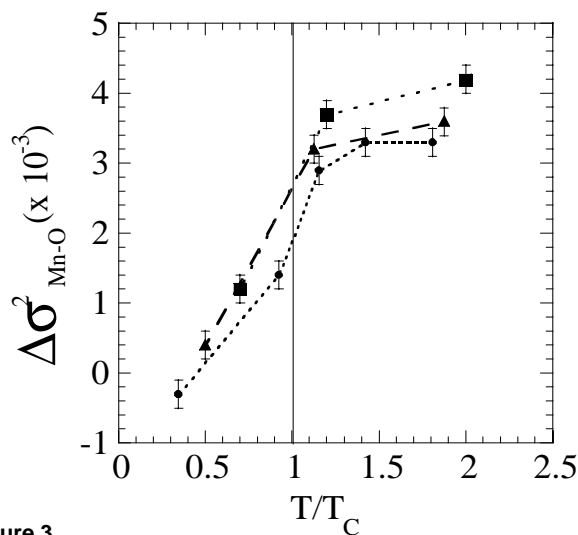


Figure 3. DW factors (relative to the CaMnO_3 DW factor) for the first coordination shell Mn-O distance of $\text{La}_{0.67}\text{Ca}_{0.33}\text{MnO}_3$ (circles), $\text{La}_{0.6}\text{Y}_{0.07}\text{Ca}_{0.33}\text{MnO}_3$ (triangles) and $\text{La}_{0.57}\text{Tb}_{0.1}\text{Ca}_{0.33}\text{MnO}_3$ (squares) samples, as a function of the reduced temperature. T_c is the Curie temperature (magnetoresistive transition).

3.2 Second shell analysis

We have also performed the structural analysis up to the second coordination shell in $\text{La}_{1-x}\text{Ca}_x\text{MnO}_3$ and $\text{Tb}_{1-x}\text{Ca}_x\text{MnO}_3$ ($x=0.5$ and 0.67) compounds, taking Mn, RE/Ca and second shell O as near-neighbour atoms. This study has been made using the program GNXAS (Filipponi *et al.*, 1995) that allows to fit the

complete EXAFS signal including multiple scattering contributions. The fit has been performed in the $3.8 \leq k \leq 12 \text{ \AA}^{-1}$ range with a theoretical signal which includes the following contribution paths: 6 Mn-O (first coordination shell), 8 $(1-x)$ Mn-RE, $8x$ Mn-Ca, 12 Mn-O (second coordination shell), 6 Mn-O-Mn and 3 Mn-O-O. Contributions of successive coordination shells up to 6 Å have been included fixing the distances and the DW factors. The different dispersion pathways have been obtained using the Pbnm orthorhombic structure of each sample. From the fitting process, we concluded that the multiple scattering Mn-O-Mn term determines the spectrum shape. Consequently, the relevant structural parameter for this study is the angle Mn-O-Mn. Fig. 4 shows the thermal evolution of the Mn-O-Mn angle for $\text{La}_{1-x}\text{Ca}_x\text{MnO}_3$ ($x=0.33, 0.5, 0.67$) and $\text{Tb}_{1-x}\text{Ca}_x\text{MnO}_3$ ($x=0.5, 0.67$) samples. The largest value for the Mn-O-Mn angle corresponds to the magnetoresistive sample ($x=0.33$). Small changes are found with varying the temperature for all the samples. However, differences are observed between magnetoresistive and charge ordering compounds. The average value of the Mn-O-Mn angle decreases by decreasing the temperature across the charge-ordering phase transition but the opposite behavior is found across the ferromagnetic transition in magnetoresistive samples.

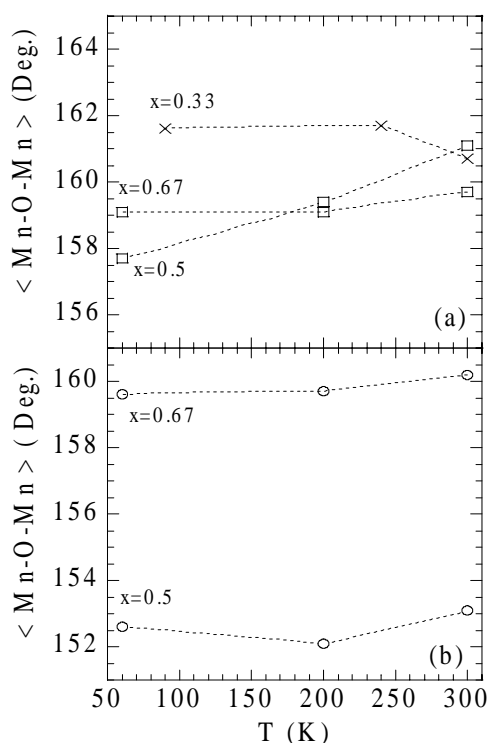


Figure 4
Thermal evolution of the average Mn-O-Mn angle ($\pm 1^\circ$) for $\text{La}_{1-x}\text{Ca}_x\text{MnO}_3$ (a) and $\text{Tb}_{1-x}\text{Ca}_x\text{MnO}_3$ (b) samples.

4. Conclusions

The extended work performed on the $\text{La}_{1-x}\text{Ca}_x\text{MnO}_3$ and $\text{Tb}_{1-x}\text{Ca}_x\text{MnO}_3$ series allows us to achieve the following conclusions, independently of the several detailed models proposed for the local distortions: (i) the room temperature local structure (paramagnetic phase) is characterised by a distribution of distorted octahedral, but the EXAFS data are not consistent with a weighted mixture of Mn^{3+} (Jahn-Teller distorted) and Mn^{4+}

(undistorted) octahedra. This point agrees with the XANES analysis which shows that these compounds can not be described by a ionic model (Subías *et al.*, 1997; García *et al.*, 2000). The distortion observed in the paramagnetic phase remains at low temperatures for non-magnetoresistive samples ($x \geq 0.5$). In some cases, the ordering of these distortions gives rise to the so-called charge-ordered phases, whereas in other cases, the random distribution of the distortions gives rise to a spin-glass behaviour, as it occurs in $\text{Tb}_{0.66}\text{Ca}_{0.33}\text{MnO}_3$. The ferromagnetic-metallic phase of the magnetoresistive samples is characterised by regular MnO_6 octahedra, being the average distortion similar to that of the CaMnO_3 sample. Therefore, the magnetoresistive transition can be described as a transition from homogeneous state to inhomogeneous state with local distortions. (ii) second coordination shell analysis has pointed out the role of the Mn-O-Mn angle on the occurrence of the metallic ferromagnetic state. The Mn-Mn electronic transfer is highly correlated to this angle and as it is known, the metallic state is achieved for larger Mn-O-Mn angles (Fontcuberta *et al.*, 1996). Therefore, the appearance of a metallic state is coupled to the increasing of the Mn-O-Mn angle. On the contrary, an insulating state (charge-ordering transition) is associated to the decreasing of the Mn-O-Mn angle.

This research was supported by the Spanish CICYT project No. MAT99-0847.

References

- Blasco J., García J., De Teresa J. M., Ibarra M. R., Pérez J., Algarabel P. A., Marquina C. & Ritter C., (1997) *J. Phys.: Condens. Matter.* **9**, 10321-10331.
- Blasco J., Ritter C., García J., de Teresa J. M., Pérez-Cacho J., & Ibarra M.R. (2000) *Phys. Rev. B*, in press.
- Booth C. H., Bridges F., Snyder G. J. & Geballe T. H. (1996). *Phys. Rev. B* **54**(22), R15606-15609.
- Booth C. H., Bridges F., Kwei G. H., Lawrence J. M., Cornelius A. L. & Neumeier J.J. (1998). *Phys. Rev. Lett.* **80**(4), 853-856.
- Booth C. H., Bridges F., Kwei G. H., Lawrence J. M., Cornelius A. L. & Neumeier J.J. (1998). *Phys. Rev. B* **57**(17), 10440-10454.
- Coe, J. M. D., Viret, M. & VonMolnar, S., (1999). *Adv. Phys.* **48**(2), 167-293.
- Filipponi A., Di Cicco A. & Natoli C. R. (1995). *Phys. Rev. B* **52**(21) 15122-15134.
- Filipponi A., Di Cicco A. & Natoli C. R. (1995). *Phys. Rev. B* **52**(21) 15135-15149.
- Fontcuberta J., Martínez B., Sefar A., Pinol S., García-Muñoz J. L. & Obradors X., (1996). *Phys. Rev. Lett.* **76**(7) 1122-1125.
- García J., Sánchez M. C., Subías G. & Blasco J., (2000). *Phys. Rev. B*. Submitted
- Ibarra M. R., de Teresa J. M., Blasco J., Algarabel P.A., Marquina C., García J., Stankiewicz J. & Ritter C., (1997). *Phys. Rev. B* **56**(13) 8252-8255.
- Lanzara A., Saini N. L., Brunelli M., Natali F., Bianconi A., Radaelli P. G. & Cheong-S-W. (1998). *Phys. Rev. Lett.* **8**(4) 878-881.
- Meneguini C., Cimino R., Pascarella S., Mobilio S., Raghu C. & Sarma D. D. (1997). *Phys. Rev. B* **56**(7) 3520-3523.
- Radaelli, P. G., Cox, D. E., Marezio, M., Cheong S-W., Schiffer, P. E. & Ramirez, A. P. (1995). *Phys. Rev. Lett.* **75**(24), 4488-4491.
- Radaelli, P.G., Cox, D. E., Marezio, M. & Cheong, S-W. (1997). *Phys. Rev. B* **55**(5), 3015-3023.
- Subías G., García J., Proietti M. G. & Blasco J. (1997) *Phys. Rev. B* **56** (13), 8183-8191.
- Subías G., García J., Blasco J. & Proietti M. G. (1998) *Phys. Rev. B* **57**(2), 748-754.
- Subías G., García J., Blasco J. & Proietti M. G. (1998) *Phys. Rev. B* **58**(14), 9287-9293.
- Tyson T. A., Mustre de León J., Conradson A. R., Bishop A. R., Neumeier J.J., Röder H. & Zang J., (1996). *Phys. Rev. B* **53**(21), 13985-13988.